An Innovative Energy Management System for Microgrids with Multiple Grid-Forming Inverters

Preprint

Joshua Comden and Jing Wang

National Renewable Energy Laboratory

Presented at the 2024 IEEE Power and Energy Society General Meeting
Seattle, Washington
July 21–25, 2024

NREL is a national laboratory of the U.S. Department of Energy
Office of Energy Efficiency & Renewable Energy
Operated by the Alliance for Sustainable Energy, LLC

This report is available at no cost from the National Renewable Energy Laboratory (NREL) at www.nrel.gov/publications.

Contract No. DE-AC36-08GO28308

Conference Paper
NREL/CP-5D00-88118
July 2024

An Innovative Energy Management System for Microgrids with Multiple Grid-Forming Inverters

Preprint

Joshua Comden and Jing Wang

National Renewable Energy Laboratory

Suggested Citation
Comden, Joshua and Jing Wang. 2024. *An Innovative Energy Management System for Microgrids with Multiple Grid-Forming Inverters: Preprint*. Golden, CO: National Renewable Energy Laboratory. NREL/CP-5D00-88118.
https://www.nrel.gov/docs/fy24osti/88118.pdf.

NREL is a national laboratory of the U.S. Department of Energy
Office of Energy Efficiency & Renewable Energy
Operated by the Alliance for Sustainable Energy, LLC

This report is available at no cost from the National Renewable Energy Laboratory (NREL) at www.nrel.gov/publications.

Contract No. DE-AC36-08GO28308

Conference Paper
NREL/CP-5D00-88118
July 2024

National Renewable Energy Laboratory
15013 Denver West Parkway
Golden, CO 80401
303-275-3000 • www.nrel.gov

NOTICE

This work was authored in part by the National Renewable Energy Laboratory, operated by Alliance for Sustainable Energy, LLC, for the U.S. Department of Energy (DOE) under Contract No. DE-AC36-08GO28308. Funding provided by U.S. Department of Energy Office of Energy Efficiency and Renewable Energy Solar Energy Technologies Office Award Number DEEE0009336.. The views expressed herein do not necessarily represent the views of the DOE or the U.S. Government.

An Innovative Energy Management System for Microgrids with Multiple Grid-Forming Inverters

Joshua Comden and Jing Wang

***Abstract*— As increasingly more grid-forming (GFM) inverter-based resources replace traditional fossil-fueled synchronous generators as the GFM sources in microgrids, the existing microgrid energy management systems (EMS) need to be updated to control and coordinate multiple GFM inverters that consider system control objectives under different microgrid connection states. For each state, we formulate an optimization problem and apply a real-time feedback-based control algorithm; altogether, the control algorithms seamlessly connect the states into a generic microgrid EMS that controls the nodal voltages and frequencies, becomes a virtual power plant (VPP) when connected to the main grid, and coordinates power sharing responsibility among GFM sources when islanded. We showcase the EMS on a real-world simulation of a microgrid under the different states to demonstrate its operational effectiveness.**

I. Introduction

An energy management system (EMS) plays a critical role in a microgrid system because it manages the control, operation, and monitoring of the whole microgrid system, including the distributed energy resources, grid assets (e.g., point of common coupling [PCC] circuit breaker, capacitor banks), and loads, and it interfaces with a distribution system operator [1]. Significant effort has been devoted to developing EMS algorithms for microgrid operation. An evolutionary adaptive dynamic programming and reinforcement learning framework is developed in [2] to dispatch grid assets in grid-connected and islanded operation. The authors of [3] developed an EMS for an islanded microgrid to manage frequency excursions from load and renewable fluctuations using information gap decision theory. A two-layer EMS is developed in [4] to adaptively manage the microgrid by defining daily directives of control strategies and operating the system in real time with all operational constraints. An EMS for short-term energy management is developed in [5] to minimize the cost of energy imports in grid-connected mode and minimize the unsupplied load in islanded mode using a global robustness approach. Another robust EMS is proposed in [6] to formulate a model predictive control for renewable uncertainties and achieve the robustness of dispatching tasks.

Multi-agent-based distributed EMS have received a lot of attention as well, such as the multi-agent-based transactive energy framework in [7] and the multi-agent-based hybrid EMS in [8]. Overall, mathematical programming, adaptive dynamic programming, deep reinforcement learning, and robust and predictive control are solutions to developing microgrid EMS while considering dynamics and capturing critical component models, stability constraints, resilient awareness, market operation, etc. [9].

With increasingly more grid-forming (GFM) inverter-based resources (IBRs) replacing traditional fossil-fueled synchronous generators as the GFM sources, the existing microgrid EMS need to be updated to control GFM inverters considering system control objectives and system and device constraints. In particular, today's GFM technology allows GFM inverters to also operate in grid-connected mode, yet there are no EMS optimally dispatching these state-of-the-art GFM inverters in grid-connected and islanded mode; therefore, the goal of this work is to bridge the aforementioned research gaps and provide a generic EMS design framework to optimally dispatch GFM inverters in grid-connected and islanded mode and to also achieve smooth transition operations. This aligns with the IEEE Std P2030.7 [10] transition and dispatch functions for microgrid controllers.

The key contributions of this paper can be summarized as follows:

1) We formulate optimization problems for the dispatch of GFM IBRs under different microgrid steady states and transition states.
2) We apply feedback-based control algorithms to each microgrid state-specific optimization problem, which generalizes the microgrid's EMS.
3) We showcase the EMS in a real-world simulation of a microgrid under the different states.

II. Microgrid Operation

A. Power System Model

Consider a microgrid with N nodes in the set $\mathcal{N} := \{1, \dots, N\}$ and the addition of node 0 as a node on the main grid to which node 1 from the microgrid connects. Let $\mathcal{G} \subset \mathcal{N}$ be the set of nodes with GFM IBRs. Nodes 0 and 1 together comprise the PCC with a circuit breaker between them. The PCC circuit breaker status is represented by the binary variable CB, where CB $= 1$ denotes that the circuit

The authors are with the Power Systems Engineering Center at the National Renewable Energy Laboratory, Golden, CO, USA. Emails: {Joshua.Comden, Jing.Wang}@nrel.gov

This work was authored by the National Renewable Energy Laboratory, operated by Alliance for Sustainable Energy, LLC, for the U.S. Department of Energy (DOE) under Contract No. DE-AC36-08GO28308. Funding provided by U.S. Department of Energy Office of Energy Efficiency and Renewable Energy Solar Energy Technologies Office Award Number DE-EE0009336. The views expressed in the article do not necessarily represent the views of the DOE or the U.S. Government. The U.S. Government retains and the publisher, by accepting the article for publication, acknowledges that the U.S. Government retains a nonexclusive, paid-up, irrevocable, worldwide license to publish or reproduce the published form of this work, or allow others to do so, for U.S. Government purposes.

breaker is closed and the microgrid is grid-connected, and CB $= 0$ denotes that the circuit breaker is open and the microgrid is islanded.

The real and reactive power injection at each node $n \in \mathcal{N}$, are denoted by P_n and Q_n, respectively. For this paper, all power injections at nodes $n \in \mathcal{N}-\mathcal{G}$ are considered noncontrollable exogenous inputs. Let $\mathbf{p} := [P_1, \ldots, P_N]$ and $\mathbf{q} := [Q_1, \ldots, Q_N]$ collect the real and reactive power injections, respectively. The voltage magnitude and frequency at each node $n \in \mathcal{N}$, are functions of the power injections and the PCC circuit breaker status, and they are denoted by $V_n(\mathbf{p}, \mathbf{q}; \text{CB})$ and $f_n(\mathbf{p}, \mathbf{q}; \text{CB})$, respectively. The voltage magnitude, V_0, and frequency, f_0, at the main grid node are given. $P_0(\mathbf{p}, \mathbf{q}; \text{CB})$ and $Q_0(\mathbf{p}, \mathbf{q}; \text{CB})$ are the real and reactive power, respectively, that flow into the microgrid from the main grid when the microgrid is grid-connected. For ease of notation and cross-nodal comparisons, all voltage magnitudes are assumed to be in per-unit scale with respect to their associated nodal nominal voltages.

B. GFM IBRs

The GFM IBRs operate in two different modes depending on the connection status of the microgrid. When the microgrid is grid-connected, they act similarly to grid-following (GFL) IBRs in PQ-control mode, where in they follow the power injection set points denoted by $(\widetilde{P}_n, \widetilde{Q}_n) \in \mathcal{S}_n$ for all nodes, $n \in \mathcal{G}$, where $\mathcal{S}_n$ is the feasible space of the power injection. Otherwise, when the microgrid is islanded, they operate in Vf-control mode, where the power injections follow the set points that push the voltage magnitudes and frequencies to references denoted by $(\widetilde{V}_n, \widetilde{f}_n)$. Thus, the functions of the power injection at node $n \in \mathcal{G}$ are:

$$P_n := \begin{cases} \widetilde{P}_n & \text{if CB} = 1 \\ \acute{P}_n(\widetilde{V}_n, \widetilde{f}_n, \mathbf{p}, \mathbf{q}) & \text{if CB} = 0 \end{cases} \tag{1a}$$

$$Q_n := \begin{cases} \widetilde{Q}_n & \text{if CB} = 1 \\ \acute{Q}_n(\widetilde{V}_n, \widetilde{f}_n, \mathbf{p}, \mathbf{q}) & \text{if CB} = 0 \end{cases} \tag{1b}$$

where the dependency of $(\acute{P}_n, \acute{Q}_n)$ on the nodal power injections $(\mathbf{p}, \mathbf{q})$ account for the GFM IBR internal control laws pushing its voltage magnitude, $V_n(\mathbf{p}, \mathbf{q}; 0)$, and frequency, $f_n(\mathbf{p}, \mathbf{q}; 0)$, to their reference set points $(\widetilde{V}_n, \widetilde{f}_n)$. It is assumes that the control laws also ensure that $(\acute{P}_n(\widetilde{V}_n, \widetilde{f}_n, \mathbf{p}, \mathbf{q}), \acute{Q}_n(\widetilde{V}_n, \widetilde{f}_n, \mathbf{p}, \mathbf{q})) \in \mathcal{S}_n : \forall(\widetilde{V}_n, \widetilde{f}_n, \mathbf{p}, \mathbf{q})$.

C. Operation States

A microgrid has different objectives depending on whether it is connected to or disconnected from the main grid and whether it is operating in a steady state or attempting to change its connection status; therefore, we define the steady-state and transition operation states of the microgrid to distinguish the different objectives.

Specifically, we denote the steady-state grid-connected state as S1 and the steady-state islanded state as S0, where 1 and 0 refer to the PCC circuit breaker status, CB. When transitioning from one steady-state to another and before closing or opening the PCC circuit breaker, we denote the transition state from grid-connected to islanded steady states as T10 and the transition state from islanded to grid-connected steady states as T01. Fig. 1 shows an overview on the progression of the operation states when disconnecting (connecting) the microgrid from (to) the main grid.

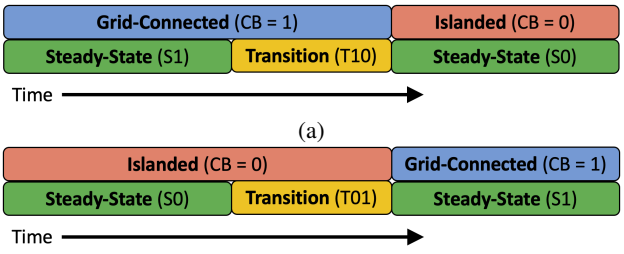

Fig. 1: Microgrid operation states when (a) disconnecting from and (b) connecting to the main grid.

III. State-Specific Problem Formulations

In this section, we formulate optimization problems under each microgrid operation state for the GFM IBR set points or references. It is implicitly inferred that the GFM IBR-related elements of $(\mathbf{p}, \mathbf{q})$ are functions of their set points or references with Eq. (1).

A. Steady-State Grid-Connected (S1)

When the microgrid is connected to the main grid, it can behave as a virtual power plant (VPP), where the IBRs collectively control the active power flowing into the microgrid, $P_0(\mathbf{p}, \mathbf{q}; 1)$, to be between $\underline{P}_{0,\text{S1}}$ and $\overline{P}_{0,\text{S1}}$, and the reactive power, $Q_0(\mathbf{p}, \mathbf{q}; 1)$, to be between $\underline{Q}_{0,\text{S1}}$ and $\overline{Q}_{0,\text{S1}}$. These bounds are typically set by a higher-level controller that is managing several microgrids, e.g., an advanced distribution management system. It is also important for the IBRs to provide voltage support to the microgrid by keeping the voltage magnitude, $V_n(\mathbf{p}, \mathbf{q}; 1)$, of each node, n, to be between the bounds $\underline{V}_n$ and $\overline{V}_n$.

With a general cost function for the normal operation of the GFM IBR at node $n \in \mathcal{G}$ being $c_{n,\text{S1}}(\widetilde{P}_n, \widetilde{Q}_n)$, we formulate the following optimization problem that minimizes the cost of operating GFM IBRs while operating the microgrid as a VPP and providing voltage support:

$$\min_{\widetilde{\mathbf{P}}, \widetilde{\mathbf{Q}}} \quad \sum_{n \in \mathcal{G}} c_{n,\text{S1}}(\widetilde{P}_n, \widetilde{Q}_n) \tag{2a}$$

$$\text{s.t.} \quad \underline{P}_{0,\text{S1}} \le P_0(\mathbf{p}, \mathbf{q}; 1) \le \overline{P}_{0,\text{S1}} \tag{2b}$$

$$\underline{Q}_{0,\text{S1}} \le Q_0(\mathbf{p}, \mathbf{q}; 1) \le \overline{Q}_{0,\text{S1}} \tag{2c}$$

$$\underline{V}_n \le V_n(\mathbf{p}, \mathbf{q}; 1) \le \overline{V}_n : \quad \forall n \in \mathcal{N} \tag{2d}$$

$$(\widetilde{P}_n, \widetilde{Q}_n) \in \mathcal{S}_n : \quad \forall n \in \mathcal{G}. \tag{2e}$$

B. Transition from Grid-Connected to Islanded (T10)

When the microgrid receives a signal from the higher-level controller to disconnect from the main grid, it prepares to be disconnected by controlling the IBRs so that the power flow into the microgrid is at or near zero. It also uses cost

functions $c_{n,\text{T10}}(\widetilde{P}_n, \widetilde{Q}_n) : \forall n \in \mathcal{G}$ that are different from the normal operation of the GFM IBRs to help facilitate a faster transition to disconnect the microgrid; thus, the optimization problem for state T10 is a modified version of Problem (2), where the cost functions are replaced with those for state T10 and $\underline{P}^t_{0,\text{T10}} = \overline{P}^t_{0,\text{T10}} = \underline{Q}^t_{0,\text{T10}} = \overline{Q}^t_{0,\text{T10}} := 0$.

C. Steady-State Islanded (S0)

When the microgrid is islanded, the GFM IBRs are responsible for being the voltage sources and regulate the frequency; the main challenge is how to best share that responsibility among them while considering their capacities.

The amount of effort that a GFM IBR contributes to maintaining the voltage is approximated by the differences between the voltage magnitude at its node and its reference value and between the frequency at its node and its reference value. That effort is discounted to account for the relative differences in capacities and control sensitivities between the GFM IBRs and then compared with the average discounted effort. This gives us the following optimization problem that works to equalize the discounted efforts' differences with their averages:

$$\min_{\widetilde{\mathbf{V}},\widetilde{\mathbf{f}}} \quad \frac{1}{2} a_{\text{S0}} \sum_{n\in\mathcal{G}} (b_{\text{V},n}(\widetilde{V}_n - V_n(\mathbf{p},\mathbf{q};0)) - e_{\text{V}}(\widetilde{\mathbf{V}},\mathbf{p},\mathbf{q}))^2 + \frac{1}{2} \sum_{n\in\mathcal{G}} (b_{\text{f},n}(\widetilde{f}_n - f_n(\mathbf{p},\mathbf{q};0)) - e_{\text{f}}(\widetilde{\mathbf{f}},\mathbf{p},\mathbf{q}))^2 \quad (3a)$$

$$\text{s.t.} \quad \underline{V}_n \le \widetilde{V}_n \le \overline{V}_n,\ \underline{f} \le \widetilde{f}_n \le \overline{f} : \quad \forall n \in \mathcal{G} \quad (3b)$$

where $a_{\text{S0}} > 0$ is a coefficient that balances the two types of efforts; $\{b_{\text{V},n}, b_{\text{f},n}\} \in (0,1]$ are the discount factors; $(\underline{f}, \overline{f})$ are the bounds on the frequency; and the average discounted efforts $(e_{\text{V}}, e_{\text{f}})$ for the voltage magnitude and frequency are defined as $e_{\text{V}}(\widetilde{\mathbf{V}},\mathbf{p},\mathbf{q}) := \frac{1}{|\mathcal{G}|}\sum_{n\in\mathcal{G}}(b_{\text{V},n}(\widetilde{V}_n - V_n(\mathbf{p},\mathbf{q};0))$ and $e_{\text{f}}(\widetilde{\mathbf{V}},\mathbf{p},\mathbf{q}) := \frac{1}{|\mathcal{G}|}\sum_{n\in\mathcal{G}}(b_{\text{f},n}(\widetilde{f}_n - f_n(\mathbf{p},\mathbf{q};0))$.

D. Transition From Islanded to Grid-Connected (T01)

When the microgrid receives a signal from the higher-level controller to connect back to the main grid, it prepares to be connected by controlling the GFM IBRs so that the voltage magnitude, frequency, and angle at Node 1 become equal to those of Node 0. This objective gives us the following optimization problem that is similar to Problem (3) for operation state S0:

$$\min_{\widetilde{\mathbf{V}},\widetilde{\mathbf{f}}} \quad \frac{1}{2} a_{\text{T01}} (V_1(\mathbf{p},\mathbf{q};0) - V_0)^2 + \frac{1}{2}((f_1(\mathbf{p},\mathbf{q};0) - f_0) + \zeta(\theta_1 - \theta_0))^2 \quad (4a)$$

$$\text{s.t.} \quad \underline{V}_n \le \widetilde{V}_n \le \overline{V}_n,\ \underline{f} \le \widetilde{f}_n \le \overline{f} : \quad \forall n \in \mathcal{G} \quad (4b)$$

where the coefficient $a_{\text{T01}} > 0$ balances the voltage magnitude and frequency objectives, $(\theta_1 - \theta_0)$ is the voltage angle difference across the PCC, and $\zeta > 0$ is a parameter that controls the sensitivity on the voltage angle difference.

IV. Microgrid Energy Management System

In this section, we apply real-time feedback-based control algorithms to the operation state-specific optimization problems described in Section III. Because the microgrid is a time-varying system, we add the time index, $t \in \mathbb{N}$, to the superscript for most variables and functions. Additionally, we use a hat on functions to represent a measured output value instead of the function itself.

A. Steady-State Grid-Connected (S1)

The control algorithm for the steady-state grid-connected state S1 applied to Problem (2) uses the primal-dual method developed in [11] and the linearization method of the power flow equations developed in [12].

Dual variables are used to guide the GFM IBRs to satisfy the constraints (2b)–(2d) through their measured violations. Specifically, the dual variables $(\underline{\lambda}_{P_0}, \overline{\lambda}_{P_0}, \underline{\lambda}_{Q_0}, \overline{\lambda}_{Q_0})$ capture the VPP violations:

$$\underline{\lambda}^{t+1}_{P_0} := \text{Proj}_{\mathbb{R}_+}\left\{\underline{\lambda}^t_{P_0} + \beta_{\text{S1}}\left(\underline{P}^t_{0,\text{S1}} - \hat{P}^t_0 - \epsilon\underline{\lambda}^t_{P_0}\right)\right\} \quad (5a)$$

$$\overline{\lambda}^{t+1}_{P_0} := \text{Proj}_{\mathbb{R}_+}\left\{\overline{\lambda}^t_{P_0} + \beta_{\text{S1}}\left(\hat{P}^t_0 - \overline{P}^t_{0,\text{S1}} - \epsilon\overline{\lambda}^t_{P_0}\right)\right\} \quad (5b)$$

$$\underline{\lambda}^{t+1}_{Q_0} := \text{Proj}_{\mathbb{R}_+}\left\{\underline{\lambda}^t_{Q_0} + \beta_{\text{S1}}\left(\underline{Q}^t_{0,\text{S1}} - \hat{Q}^t_0 - \epsilon\underline{\lambda}^t_{Q_0}\right)\right\} \quad (5c)$$

$$\overline{\lambda}^{t+1}_{Q_0} := \text{Proj}_{\mathbb{R}_+}\left\{\overline{\lambda}^t_{Q_0} + \beta_{\text{S1}}\left(\hat{Q}^t_0 - \overline{Q}^t_{0,\text{S1}} - \epsilon\overline{\lambda}^t_{Q_0}\right)\right\} \quad (5d)$$

where $\beta_{\text{S1}} > 0$ is the step size, and $\epsilon > 0$ is a regularization parameter. Similarly, the dual variables $(\underline{\nu}_n, \overline{\nu}_n)$ capture the voltage support violations at each node $m \in \mathcal{N}$:

$$\underline{\nu}^{t+1}_m := \text{Proj}_{\mathbb{R}_+}\left\{\underline{\nu}^t_m + \gamma\left(\underline{V}_m - \hat{V}_m - \epsilon\underline{\nu}^t_m\right)\right\} \quad (6a)$$

$$\overline{\nu}^{t+1}_m := \text{Proj}_{\mathbb{R}_+}\left\{\overline{\nu}^t_m + \gamma\left(\hat{V}_m - \overline{V}_m - \epsilon\overline{\nu}^t_m\right)\right\} \quad (6b)$$

where $\gamma > 0$ is the voltage support step size. The dual variables are combined into power injection directions $(h_{P,n}, h_{Q,n})$ for each node $n \in \mathcal{G}$:

$$h^t_{P,n} := (\underline{\lambda}^t_{P_0} - \overline{\lambda}^t_{P_0})D_{P_0,n} + (\underline{\lambda}^t_{Q_0} - \overline{\lambda}^t_{Q_0})D_{Q_0,n} + \sum_{m\in\mathcal{N}}(\underline{\nu}^t_m - \overline{\nu}^t_m)A_{n,m} \quad (7a)$$

$$h^t_{Q,n} := (\underline{\lambda}^t_{P_0} - \overline{\lambda}^t_{P_0})E_{P_0,n} + (\underline{\lambda}^t_{Q_0} - \overline{\lambda}^t_{Q_0})E_{Q_0,n} + \sum_{m\in\mathcal{N}}(\underline{\nu}^t_m - \overline{\nu}^t_m)B_{n,m} \quad (7b)$$

where $(D_{P_0,n}, D_{Q_0,n}, E_{P_0,n}, E_{Q_0,n})$ and $(A_{n,m}, B_{n,m})$ are the coefficients from the linearized power flow equations.

The GFM IBR power injection set points $(\widetilde{P}_n, \widetilde{Q}_n)$ are set by moving in the gradient descent direction of its cost function and the power injection directions $(h_{P,n}, h_{Q,n})$:

$$\begin{bmatrix}\widetilde{P}^{t+1}_n \\ \widetilde{Q}^{t+1}_n\end{bmatrix} := \text{Proj}_{\mathcal{S}^t_n}\left\{\begin{bmatrix}\widetilde{P}^t_n \\ \widetilde{Q}^t_n\end{bmatrix} - \alpha_n\left(\nabla c^t_{n,\text{S1}}(\widetilde{P}^t_n, \widetilde{Q}^t_n) - \begin{bmatrix}h^t_{P,n} \\ h^t_{Q,n}\end{bmatrix} + \kappa\begin{bmatrix}\widetilde{P}^t_n \\ \widetilde{Q}^t_n\end{bmatrix}\right)\right\} \quad (8)$$

where $\alpha_n > 0$ is a step size, and $\kappa > 0$ is a regularization parameter.

B. Transition From Grid-Connected to Islanded (T10)

Because the optimization problem for state T10 is a modified version of Problem (2) for state S1, the control algorithm for state T10 follows Eqs. (5)–(8) with some minor modifications. All references to state S1 are changed to state T10, all VPP bounds are set to zero, i.e., $\underline{P}^t_{0,\text{T10}} = \overline{P}^t_{0,\text{T10}} = \underline{Q}^t_{0,\text{T10}} = \overline{Q}^t_{0,\text{T10}} := 0$, and the T10 VPP step size, β_{T10}, should be larger than that of state S1 so that the power flow across the PCC quickly becomes near zero. The PCC circuit breaker should be opened only when the power flow across the PCC is below a threshold; however, special care must be taken at this moment to lessen transients and the chance for instability. From experience, the best way to avoid these issues is to hold all set points and references constant right before and right after opening the PCC circuit breaker.

C. Steady-State Islanded (S0)

To control the voltage magnitude and frequency references of the GFM IBRs when the microgrid is in steady-state islanded state, we take a descending gradient step of the objective function of Problem (3) with voltage measurements and project it onto the constraint set:

$$\widetilde{V}_n^{t+1} := \text{Proj}_{[\underline{V}_n, \overline{V}_n]}\Big\{\widetilde{V}_n^t - \eta_{\text{V},n}\frac{|\mathcal{G}|-1}{|\mathcal{G}|}a_{\text{S0}}b_{\text{V},n}(\widetilde{V}_n^t - \hat{V}_n^t - \widetilde{e}_{\text{V}}^t)\Big\}$$

$$\widetilde{f}_n^{t+1} := \text{Proj}_{[\underline{f}_n, \overline{f}_n]}\Big\{\widetilde{f}_n^t - \eta_{\text{f},n}\frac{|\mathcal{G}|-1}{|\mathcal{G}|}b_{\text{f},n}(\widetilde{f}_n^t - \hat{f}_n^t - \widetilde{e}_{\text{f}}^t)\Big\}$$

where $\eta_{\text{V},n} > 0$ and $\eta_{\text{f},n} > 0$ are step sizes, $\widetilde{e}_{\text{V}}^t := \frac{1}{|\mathcal{G}|}\sum_{n\in\mathcal{G}}(b_{\text{V},n}(\widetilde{V}_n - \hat{V}_n^t)$, and $\widetilde{e}_{\text{f}}^t := \frac{1}{|\mathcal{G}|}\sum_{n\in\mathcal{G}}(b_{\text{f},n}(\widetilde{f}_n - \hat{f}_n^t)$.

D. Transition from Islanded to Grid-Connected (T01)

The gradient descent method is used on Problem (4), similar to state S0, to prepare the microgrid to reconnect to the main grid:

$$\widetilde{V}_n^{t+1} := \text{Proj}_{[\underline{V}_n, \overline{V}_n]}\{\widetilde{V}_n^t - \rho_{\text{V},n}a_{\text{T01}}(\hat{V}_1^t - \hat{V}_0^t)\}$$

$$\widetilde{f}_n^{t+1} := \text{Proj}_{[\underline{f}_n, \overline{f}_n]}\{\widetilde{f}_n^t - \rho_{\text{f},n}((\hat{f}_1^t - \hat{f}_0^t) + \zeta(\hat{\theta}_1^t - \hat{\theta}_0^t))\}$$

where we approximate that the derivatives of $V_1(\mathbf{p}, \mathbf{q}; 0)$ with respect to $\widetilde{V}_n$ and $f_1(\mathbf{p}, \mathbf{q}; 0)$ with respect to $\widetilde{f}_n$ are both 1. The microgrid should be reconnected to the main grid only when the voltage magnitude, angle, and frequency differences across the PCC are below the predefined thresholds. Similar to state T10, transients can be lessened by holding all set points and references constant right before and after closing the PCC circuit breaker.

V. Numerical Evaluation

To validate the proposed innovative EMS, an example microgrid is used for the validation. This microgrid is Feeder 2 of the benchmark Banshee model, and the single-line diagram is presented in Fig. 2. This is a 100% renewable

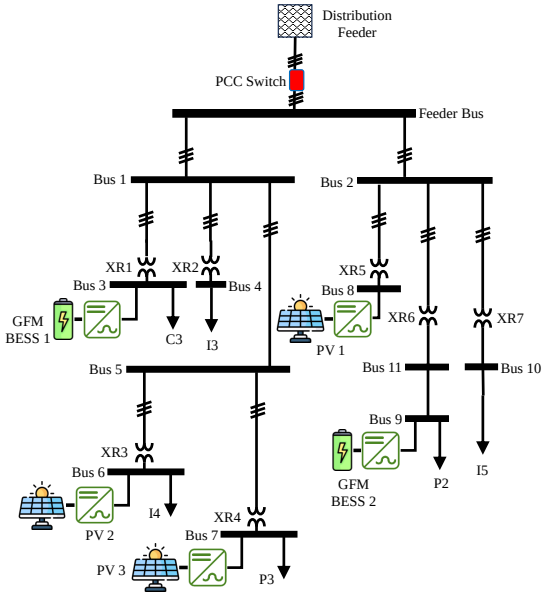

Fig. 2: Example microgrid under study.

microgrid that has two GFM battery inverters (BESS 1 2 MVA and BESS 2 1 MVA) and three PV inverters (PV 1 2 MVA, PV 2 1 MVA, and PV 3 0.5 MVA), and the peak load is 4.6 MVA. The GFM inverters always operate in GFM control, and the active and reactive power references are dispatched in grid-connected mode. The PV inverters have three operation modes: fixed power factor, volt-var, and external P and Q dispatch. For the load, "C" stands for critical load, "P" stands for priority load, and "I" stands for interruptible load. More details on this microgrid can be found in [13]. The microgrid model and the EMS were developed in MATLAB/Simulink running at 50 μs.

The EMS demonstration goes through all four operation states within a 35-second simulation, starting in S1; the states are partitioned and labeled in the figures. Fig. 3a displays the VPP bounds and the active power flow across the PCC, which shows that the EMS can follow the VPP bounds, especially when entering state T10 to prepare the microgrid for islanding. Fig. 3b gives the voltage magnitudes at all the nodes within the microgrid and shows that the voltages have very few transients when moving between the different states. The three-phase current flow across the PCC is shown in Fig. 3c when the circuit breaker is opened and in Fig. 3d when it is closed. We also note that the conditions for islanding during state T10 were met within 2 seconds and the conditions for connecting back to the main grid during state T01 were met within 7 seconds which demonstrates fast transition capabilities. The set points and references for the BESS and PV units are given in Fig. 4 for their relevant states, which shows their smooth trajectories, especially when the PCC circuit breaker is opened or closed.

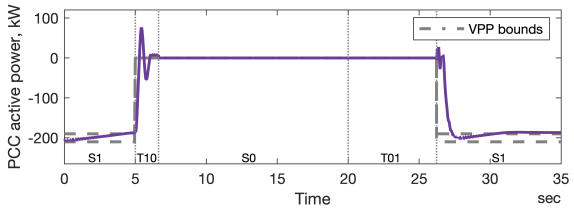

(a) VPP

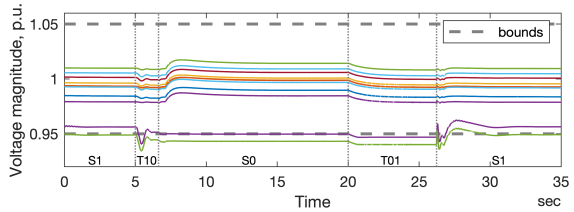

(b) Voltage support

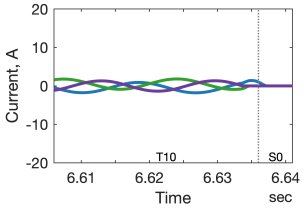

(c) PCC current flow - T10

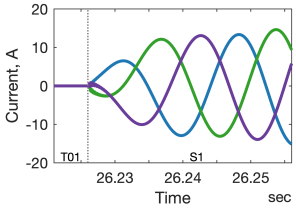

(d) PCC current flow - T01

Fig. 3: (a) Active power flow across the PCC with VPP bounds, (b) voltage magnitudes at all nodes in the microgrid, and the three-phase current flow accross the PCC during (c) T10 and (d) T01.

VI. Conclusion

In this paper, we develop a generic microgrid EMS that seamlessly dispatches GFM IBRs under the different connection states of the microgrid. The EMS is based on the application of real-time feedback-based control algorithms on microgrid optimization problems that account for the different operational objectives for each state. The EMS was numerically simulated on a real-world microgrid and demonstrated its ability to smoothly move from one state to the next. Future research directions include integrating GFL IBRs to support the GFM IBRs and testing the EMS on a microgrid in the field.

References

[1] J. Wang, C. Zhao, A. Pratt, and M. Baggu, "Design of an advanced energy management system for microgrid control using a state machine," *Applied Energy*, vol. 228, pp. 2407–2421, 2018.

[2] G. K. Venayagamoorthy, K. R. Sharma, K. P. Gautam, and A. Ahmadi, "Dynamic energy management system for a smart microgrid," *IEEE Tran. Nueral Networks and Learning Systems*, vol. 27, no. 8, pp. 1643–1656, 2016.

[3] N. Rezaei, A. Ahmadi, H. A. Khazali, and M. J. Guerrero, "Energy and frequency hierarchical management system using information gap decision theory for islanded microgrids," *IEEE Tran. Industrial Electronics*, vol. 65, no. 10, pp. 7921–7932, 2018.

[4] A. Hooshmand, B. Asghari, and K. R. Sharma, "Experimental demonstration of a tiered power management system for economic operation of grid-tied microgrids," *IEEE Tran. Sustainable Energy*, vol. 5, no. 4, pp. 1319–1327, 2014.

[5] S. J. Giraldo, A. J. Castrillon, C. J. Lopez, J. M. Rider, and A. C. Castro, "Microgrids energy management using robust convex programming," *IEEE Tran. Smart Grid*, vol. 10, no. 4, pp. 4520–4530, 2019.

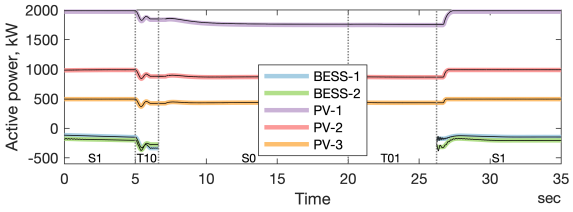

(a) Active power set points

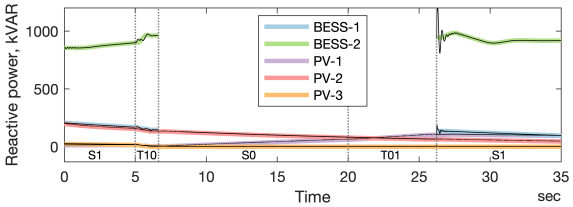

(b) Reactive power set points

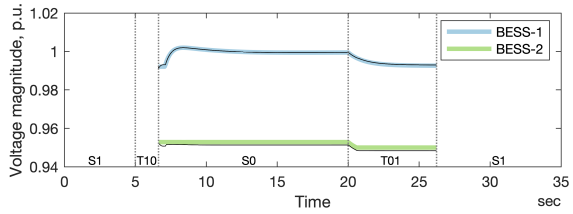

(c) Voltage magnitude references

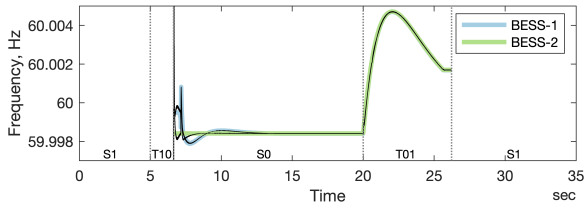

(d) Frequency references

Fig. 4: IBR set points and references: (a) active and (b) reactive power set points, and (c) voltage magnitude and (d) frequency references. The black lines are the actual values.

[6] F. Valencia, J. Collado, D. Saez, and G. L. Marin, "Robust energy management system for a microgrid based on a fuzzy prediction interval model," *IEEE Tran. Smart Grid*, vol. 7, no. 3, pp. 1486–1494, 2016.

[7] H. S. V. S. K. Nunna and D. Srinivasan, "Multiagent-based transactive energy framework for distribution systems with smart microgrids," *IEEE Tran. Ind. Informatics*, vol. 13, no. 5, pp. 2241–2250, 2017.

[8] M. Mao, P. Jin, D. N. Hatizargyriou, and L. Chang, "Multiagent-based hybrid energy management system for microgrids," *IEEE Tran. Sustainable Energy*, vol. 5, no. 3, pp. 938–946, 2014.

[9] X. Liu *et al.*, "Microgrid energy management with energy storage systems: A review," *CSEE Journal of Power and Energy Systems*, vol. 9, no. 2, pp. 483–504, 2023.

[10] "Ieee standard for the specification of microgrid controllers," *IEEE Std 2030.7-2017*, pp. 1–43, 2018.

[11] A. Bernstein and E. Dall'Anese, "Real-time feedback-based optimization of distribution grids: A unified approach," *IEEE Transactions on Control of Network Systems*, vol. 6, no. 3, pp. 1197–1209, 2019.

[12] A. Bernstein and E. Dall'Anese, "Linear power-flow models in multiphase distribution networks," in *2017 IEEE PES Innovative Smart Grid Technologies Conference Europe (ISGT-Europe)*, pp. 1–6, IEEE, 2017.

[13] J. Wang, "Study of inverter control strategies on the stability of microgrids toward 100% renewable penetration," in *IECON 2022 – 48th Annual Conference of the IEEE Industrial Electronics Society*, pp. 1–6, IEEE, 2022.